International Society for Rock Mechanics and Rock Engineering
Norwegian Group for Rock Mechanics

ISRM International Symposium
Eurock 2025 – Expanding the Underground Space
Trondheim, Norway, 16-20 June
ISBN 978-82-8208-079-8

Comparative Analysis of Multiple Mining Schemes for Large-Scale Deep Iron Ore Mines

Haoyan Wu, Yuming Liu, Ruijun Zhu, Wen li, Aimin Zhang
China ENFI Engineering Corporation, Beijing, China
wuhaoyan@live.cn

Abstract

Iron ore deposits are typically characterized by substantial reserves and relatively simple geological configurations. However, deep mining of thick iron ore bodies presents critical ground control challenges that demand sophisticated engineering solutions, particularly compared to shallow mining operations. This study investigates the stability of large-scale deep mining through a comprehensive numerical analysis using FLAC3D 9.0. A representative Chinese iron mine was modeled in three dimensions, incorporating user-defined FISH functions to systematically evaluate level segmentation, panel organization, and stope structural parameters. Four distinct mining schemes were simulated to comparatively analyze stress evolution patterns and pillar deformation behavior, including horizontal and inter-panel pillar responses. Results demonstrate that vertical pillar displacement correlates nonlinearly with both panel span and inter-pillar width, while stress concentration factors at pillar intersections range from 1.1 to 1.2. Ultimately, an optimal plan for efficient and continuous collaborative mining in large-scale deep-mining regions was determined. These findings provide actionable insights for designing safe and efficient mining strategies in analogous deep-seated iron ore deposits.

Keywords

Deep mining, Iron mine, inter-panel pillar, FLAC3D simulation, Numerical modeling

ISRM

NBG

1 Introduction

In deep iron ore mining, strategic pillar retention and panel parameter optimization constitute critical engineering considerations for mine safety, resource recovery enhancement, and cost reduction. As global mineral resources become increasingly depleted and the mining depth extend, the challenges faced by deep mining also become more severe, including high original rock temperatures, high in-situ stresses, rock bursts, and pillar stability issues. Interval panel pillars, a vital part of mine support structures, are not only related to mine stability and miner safety but also directly impact the rational utilization of mineral resources and economic benefits (Zhao, X. and Zhou, X., 2022; Zhou, X. et al, 2023).

Rationally retaining ore pillars is an effective means of controlling ground pressure activities in deep mining. It helps to adjust the stress concentration in the void and surrounding rock. Contemporary approaches to pillar design combine empirical engineering methods with theoretical calculations (Qian, J. and Xu, W., 2024; Andrade, L. and Dimitrakopoulos, R., 2024). The emergence of advanced numerical modeling techniques, particularly three-dimensional finite difference methods, has significantly enhanced engineering analysis capabilities (Zhang, Q. and Huang, M. 2024; Saadat, M. etal. 2024). This study contributes to this technological progression through systematic FLAC3D modeling of pillar behavior under multiple mining scenarios.

The stability of the mining field in underground mining includes the stability of ore pillars and the roof stability of mining stopes. In the first mining section, after the ore is mined out, the overlying rock of the void loses direct support, and the self-weight stress is transferred to the ore pillars on both sides of the void, causing stress concentration in the ore pillars and creating a stress relief area in the roof. The roof of the goaf is subjected to the pressure of its own weight and the overlying rock, and squeezes and deforms towards the goaf, that is, the roof subsides. Tensile stress may be generated, and when it exceeds the tensile strength limit of the rock, the roof will fracture.

Structural parameter optimization of mining panels involves the scientific determination of the best pillar size, shape, and layout to maximize the amount of ore extracted and minimize mining costs while ensuring safety. This process requires a comprehensive consideration of various factors such as geological conditions, rock mechanics properties, mining technology, and economic factors. Traditional pillar design methods often rely on experience and lack systematic scientific basis, while the application of modern numerical simulation technology, especially software like FLAC3D, provides more accurate and efficient tools for pillar design.

A case study was performed on the optimization of stope parameters in China. FLAC3D 9.0 was utilized in this study. Its computational capabilities enable relatively efficient calculations for large - scale models with nearly ten million grids, which provides a useful tool for this research. By creating more realistic ore body models, stope structure layouts, and simulating mining sequences, it is possible to gain insights that can contribute to the design and guidance of actual mine construction and production. These simulations help in understanding the complex interactions between different factors in the mining process, such as stress distribution, rock deformation, and stability of the mining field. However, it should be noted that while numerical simulations are valuable, they are approximations of real - world conditions, and their results need to be carefully evaluated and verified in combination with field data and engineering experience.

2 Background

2.1 Mining district

Chen Tai Gou Iron Mine is a large-scale concealed ore deposit. There are seven ore bodies in the area, and the main ore body, Fe1, constitutes 99% of the total ore deposit resources. The Fe1 ore body extends throughout the area, and all ore types are magnetite lean ores. The ore body is thick and layered, with an overall strike of around 330°, a dip to the northeast of about 60°, and a dip angle of 65 to 71°. The controlled elevation is from -660 to -1567 meters, and the stored elevation is from -647 to -1751 meters, with a burial depth of 692 to 1798 meters. The true thickness of the orebody ranges from 81.99 meters to 271.20 meters, with an average true thickness of 202.80 meters, and the thickness variation is stable.

The mine will adopt the open stoping mining method with cemented tailings backfilling. For the bottom 8m and top 5m of the first and second mining stopes, a backfill with a ratio of 1:8 of bond material to tailings by weight is used, with a strength of not less than 3MPa; the middle part of the first mining stope is backfilled with a backfill material with a ratio of 1:10, with a strength of not less than 2.5 MPa, and the middle part of the second mining stope is backfilled with a backfill material with a ratio of 1:20.

2.2 In-situ stress

Chen Tai Gou Iron Mine is characterized by a substantial burial depth and elevated in - situ stress levels. The principal orientation of the maximum horizontal principal stress within the mining area lies between N52° and 69°. Notably, this direction is approximately perpendicular to the strike of the ore body, indicating that the overall in - situ stress field in the mining area is predominantly governed by tectonic stress.

During the first-phase mining operation, the maximum horizontal principal stress fluctuates within the range of 22MPa to 33MPa, while the minimum horizontal principal stress varies from 12MPa to 18MPa. This places the mining area within a medium-high in-situ stress regime, presenting a minor risk of rock bursts during the extraction process. In the second-phase mining, the stress conditions become more severe. The maximum horizontal principal stress increases to a range of 33MPa to 54MPa, and the minimum horizontal principal stress rises to 19MPa to 33MPa, classifying the area as a high in - situ stress field.

According to the research data of the mining area, the maximum principal stress in the Chen Tai Gou mining area is identified as the horizontal tectonic stress, with its direction precisely at NE52°, forming a perpendicular angle to the ore body's strike. In the numerical model, a stepped in - situ stress distribution is applied, which increases proportionally with the depth. The formula used to calculate the in - situ stress in the mining area is presented in Equation (1).

$$\begin{cases} \sigma_{h,max} = 0.0313H - 0.0634 \\ \sigma_{h,min} = 0.0169H + 0.4011 \\ \sigma_v = 0.026H - 0.0325 \end{cases} \tag{1}$$

Where $\sigma_{h,max}$ Maximum horizontal principal stress
$\sigma_{h,min}$ Minimum horizontal principal stress
σ_v Vertical principal stress
H Burial depth of the ore body

This set of equations provides a quantitative basis for accurately simulating and analyzing the stress state during the mining process, which is crucial for ensuring the stability of the mining environment and the safety of mining operations.

2.3 Mining sequence

Chen Tai Gou Iron Mine is designed with an annual production capacity of 11 million tons per year. The first phase of the project mines the ore bodies between -620m and -1020m, and the second phase of the project mines the ore bodies between -1020m and -1754m. To ensure the stability of the mining area while reducing the impact of underground mining on the surface, intermediate pillars are retained within the mining panels and between the mining panels. A 20m thick isolation safety ore pillar is retained between the upper and lower mining areas of the first phase and between the first and second phases of the project, which are named as No.1 horizontal ore pillar and No.2 horizontal ore pillar; a 30m thick isolation safety ore pillar named No.3 is retained between the upper and lower mining areas of the second phase; a 40m thick isolation safety ore pillar named No.4 is retained between the mining of ore bodies above -1660m and below -1660m in the second phase.

The first phase is designed to mine the upper and lower mining areas simultaneously, that is, the -780m level and the -1020m level are mined at the same time, both adopting a bottom-up mining sequence. The upper mining area sequentially mines the -780m and -700m levels, while the lower mining area mines the -1020m, -940m, and -860m levels in one go. The second phase mines the ore bodies between -1020m and -1754m, first mining the ore bodies between -1020m and -1660m, and finally mining the ore bodies between -1660m and -1754m. The ore bodies between -1020m and -1660m are mined with a simultaneous bottom-up sequence in both the upper and lower mining areas. The upper mining area sequentially mines the -1340m, -1280m, -1220m, -1160m, and -1100m levels, while the lower mining area sequentially mines the -1660m, -1600m, -1540m, -1480m, and -1420m levels. For the mining of ore bodies between -1660m and -1754m, only the -1754m level is set.

3 Simulations

3.1 Model construction

The ore body's geological model is imported into FLAC3D and partitioned into different groups, including surrounding rock, ore body, horizontal ore pillars, and vertical intermediate pillars. The model dimensions are 6400m in the x-axis direction (ore body strike), 1856m in the y-axis direction (perpendicular to the ore body strike), and 2200m in the z-axis direction, generating over 8 million grid cells. The model is shown in Figure 1.

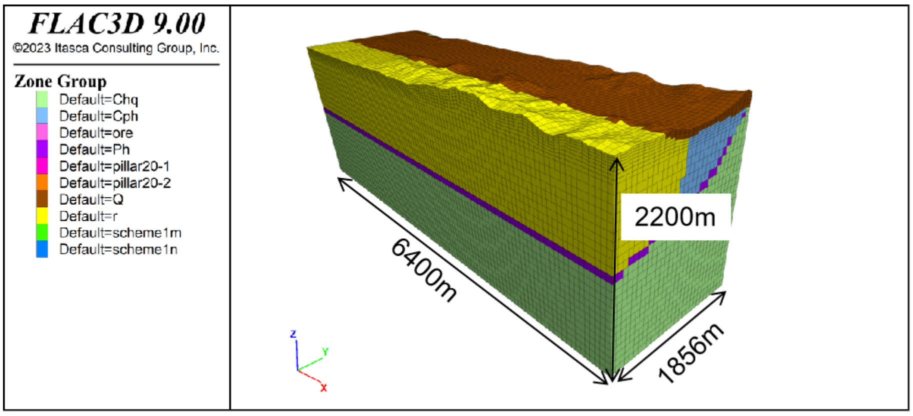

Fig. 1 model groups

Table 1 presents four different stope structure schemes.

Table 1 four different stope structure schemes

	left inter-panel pillar width	stoping panel width	right inter-panel pillar width
scheme1	20m	60m	20m
scheme2	14m	60m	26m
scheme3	22m	70m	30m
scheme4	26m	90m	34m

Under different mining structure layouts, the mining field is excavated. This is done to analyze the distribution and changes of displacement, stress, and plastic zones around the ore pillars after the mining field has been mined. To facilitate the comparison of monitoring results, monitoring points at different levels are set up in the mining field section. For example, at the -790m, -1030m, -1350m, and -1680m levels, three monitoring points are set up in two vertical intermediate pillars and horizontal ore pillars, respectively. At the -830m, -900m, and -980m levels, three monitoring points are set up in two vertical intermediate pillars and in the middle of the mining field, respectively.

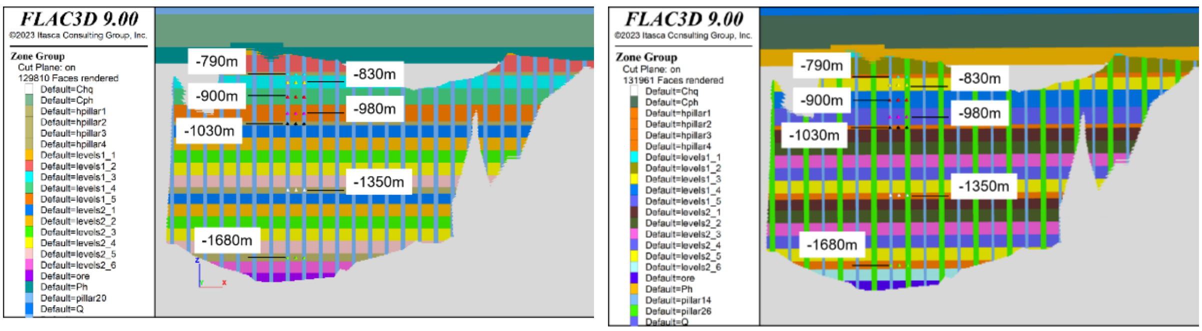

(a) scheme1 (b) scheme2

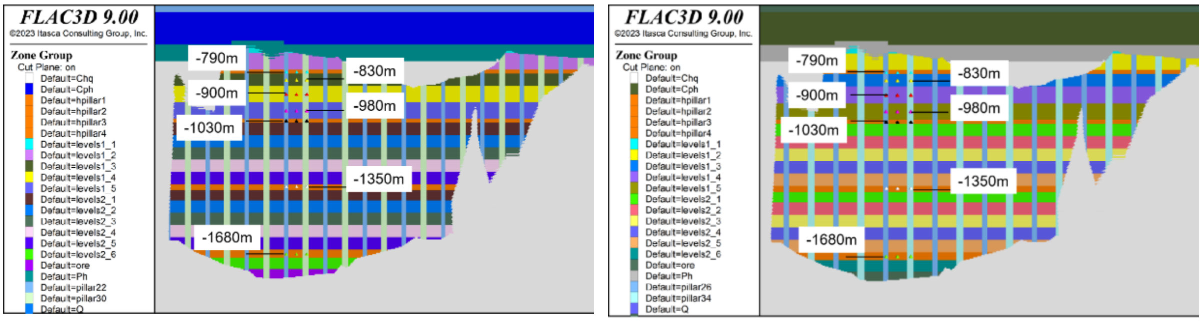

(c) scheme3 (d) scheme4

Fig. 2 display of monitoring points for different schemes

The initial stress simulation results are shown in Figure 3.

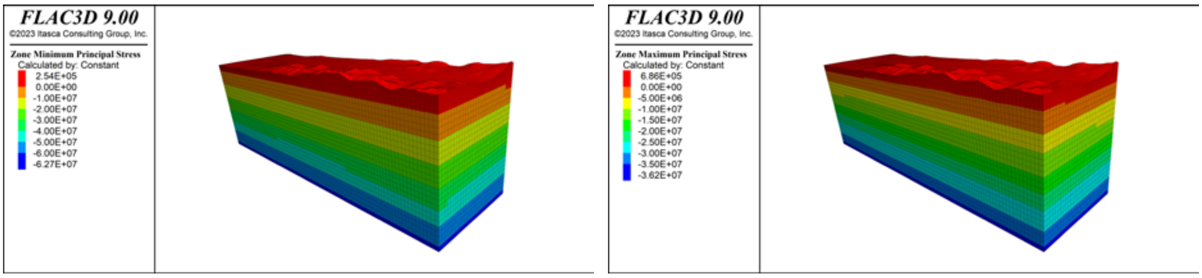

(a) Minimum Principal Stress (b) Maximum Principal Stress

Fig. 3 initial stress

The Mohr-Column constitutive model is employed for this study. The physical and mechanical parameters of the rock mass utilized in the numerical simulation are presented in Table 2, while the sequences of the numerical simulation mining operations are detailed in Table 3.

Table 2 rock mass physical and mechanical parameters

lithology	**Unit weight [kN/m^3]**	**Tensile strength [MPa]**	**Deformation modulus** [GPa]	**Poisson's ratio**	**Cohesion [MPa]**	**Angle of friction[°]**
Sericite Quartz	28.5	0.93	11	0.28	1.1	44
Carbonaceous Phyllite	27.8	0.97	12	0.27	1.2	46
Chlorite Schist	27.3	1.15	29	0.21	2.0	58
Iron ore	35.2	1.34	33	0.20	2.5	60
Chlorite Phyllite	27.7	0.75	7	0.29	0.8	40
gneissose granite	28.0	1.10	22	0.23	1.7	54

Table 3 numerical simulation mining sequences

steps	**mining area**	**steps**	**mining area**
1	level -780m~-700m, level -1020m~-940m	6	Level -1220m~-1160m, Level -1540m~-1480m
2	level -700m~-620m, level -940m~-860m	7	Level -1160m~-1100m, Level -1480m~-1420m
3	level -860m~-780m	8	Level -1100m~-1040m, Level -1420m~-1360m
4	level -1340m~-1280m, level -1660m~-1600m	9	Level -1700m~-1754m
5	level -1280m~-1220m, level -1600m~-1540m		

3.2 Results analysis

This section conducts a comprehensive discussion and in-depth analysis of the numerical simulation results through multiple means, such as displacement monitoring curves, cross-sectional views of stress redistribution, and cross-sectional views of plastic zone distribution .

3.2.1 Displacement

Based on the monitoring points shown in Figure 2, the vertical displacements of the four horizontal ore pillars and the horizontal displacements of the inter-panel pillars are presented in Figures 4-7.

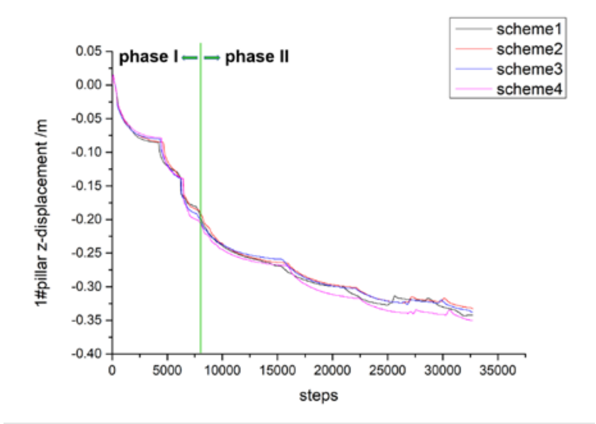

(a) No. 1 horizontal ore pillar(-790m)

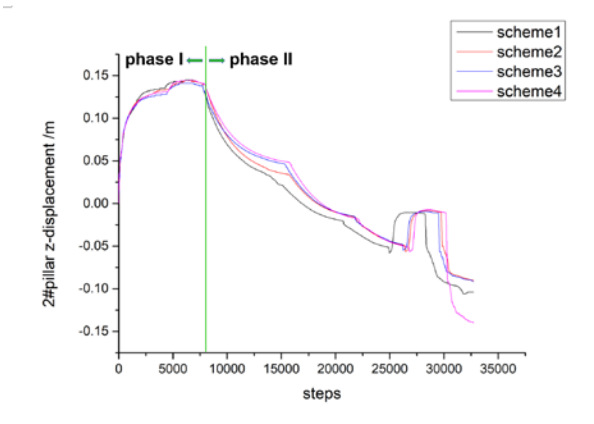

(b) No. 2 horizontal ore pillar(-1030m)

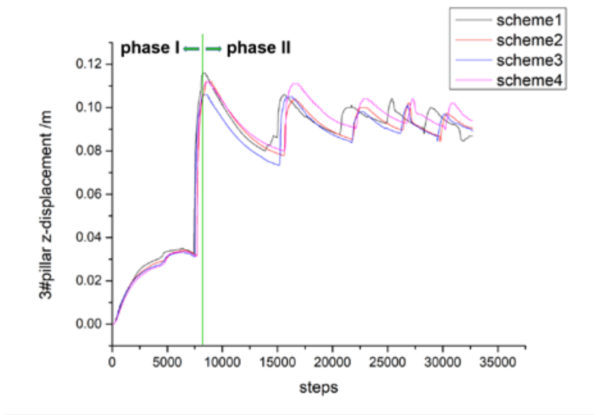

(c) No. 3 horizontal ore pillar(-1350m)

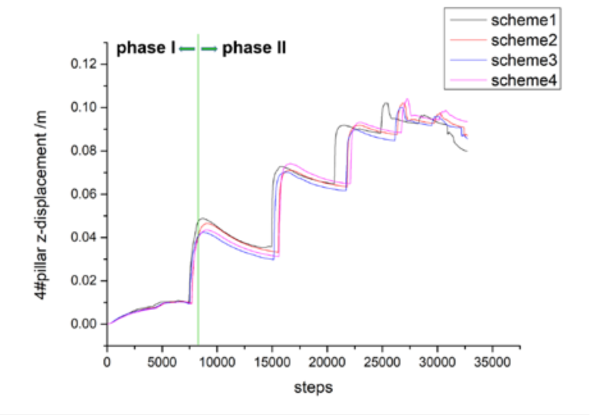

(d) No. 4 horizontal ore pillar(-1680m)

Fig. 4 vertical displacement of horizontal pillars

As depicted in Figure 4, The No. 1 horizontal ore pillar mainly experiences settlement. The No. 2 horizontal ore pillar shows uplift in Phase I and settlement in Phase II. Both the No. 3 and No. 4 horizontal ore pillars are mainly characterized by uplift. Among the four schemes, Scheme 4 shows the greatest vertical displacement, likely due to its 90m panel span. However, the vertical displacement of the horizontal ore pillars is not solely determined by the panel span. For instance, in Scheme 3, although the panel span is 70m, its vertical displacement is relatively smaller than that of a 60m-span panel in some cases. This indicates that the width of the inter-panel pillars also has a non-neligible impact on the vertical displacement of the horizontal ore pillars.

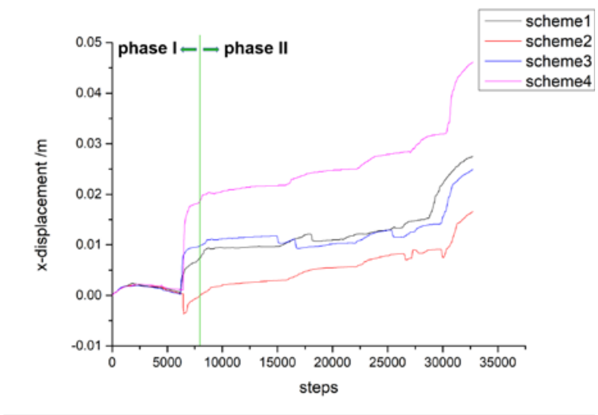

(a) left pillar

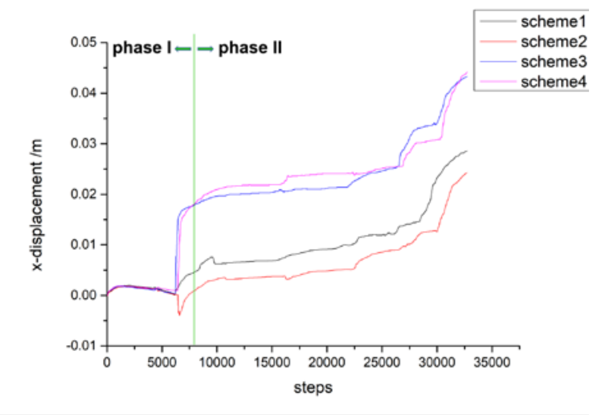

(b) right pillar

Fig.5 x-displacement of inter-panel pillar(-830m)

Regarding the horizontal displacement of the inter - panel pillars, as shown in Figure 5(a), in Scheme 4, the left inter-panel pillar (26m wide) has the maximum x-direction displacement, reaching approximately 45mm. It is followed by Scheme 1 (20m wide), Scheme 3 (22m wide), and Scheme 2 (14m wide) with the smallest displacement. Figure 5(b) shows that in Scheme 4, the right inter-panel pillar (34m wide) has the maximum x-direction displacement, and Scheme 3 (30m wide) has a displacement not much different, both around 45mm. Scheme 1 (20m wide)comes next, and Scheme 2 (26m wide) has the minimum x-direction displacement. Overall, the horizontal displacement of the inter-panel pillars is the smallest in Scheme 2.

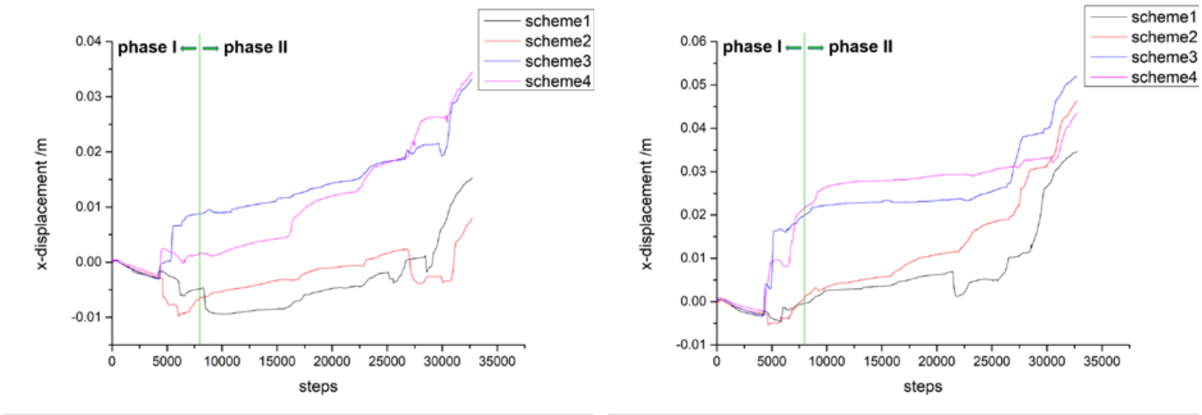

(a) left pillar (b) right pillar

Fig.6 x-displacement of inter-panel pillar(-900m)

Similar trends can be observed in Figure 6 and 7 at different levels. In Figure6(a), in Scheme 4, the left panel interval pillar (26m wide) has the maximum x-direction displacement of about 35mm, followed by Scheme 3 (22m wide), Scheme 1 (20m wide), and Scheme 2 (14m wide) with the minimum. In Figure6(b), the right inter-panel pillar in Scheme3(30m wide) has the largest x-direction displacement, followed by Scheme 2 (26m wide), Scheme 4 (34m wide), and Scheme 1 (20m wide) with the smallest.

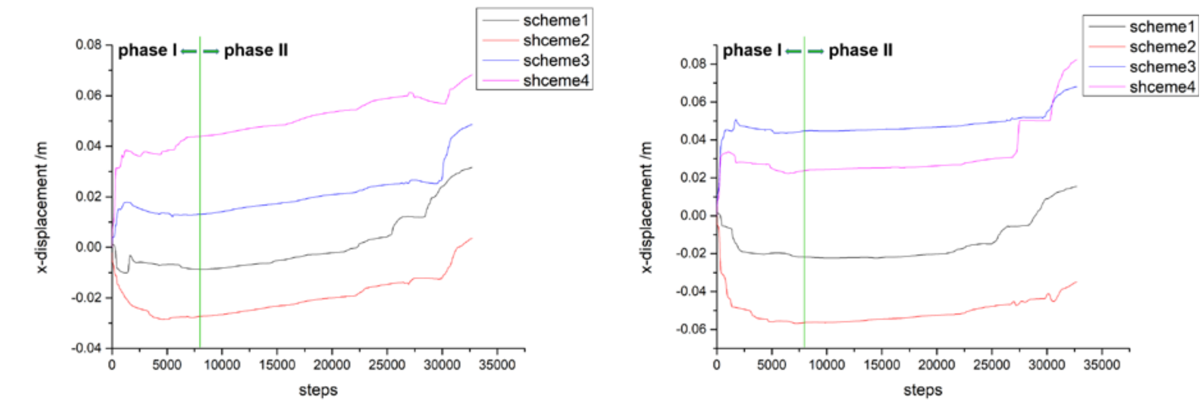

(a) left pillar (b) right pillar

Fig.7 x-displacement of inter-panel pillar(-980m)

In Figure 7(a), in Scheme 4, the left inter-panel pillar (26m wide) has the maximum x-direction displacement of approximately 62mm, followed by Scheme 3 (22m wide), Scheme 1 (14m wide), and Scheme 2 (20m wide) with the smallest. In Figure 7(b), the right panel interval pillar (34m wide) in Scheme 4 has the maximum x-direction displacement, followed by Scheme 3 (30m wide), Scheme2 (26m wide), and Scheme 1 (20m wide) with the minimum.

3.2.2 Stress redistribution

Figure 8 presents cross-section views along the dip of the ore body to study the stress redistribution after mining and backfilling are completed. Stress concentration occurs at the intersection points of the horizontal ore pillars and the vertical pillars in the panel areas. Notably, this stress concentration becomes more prominent with increasing depth.

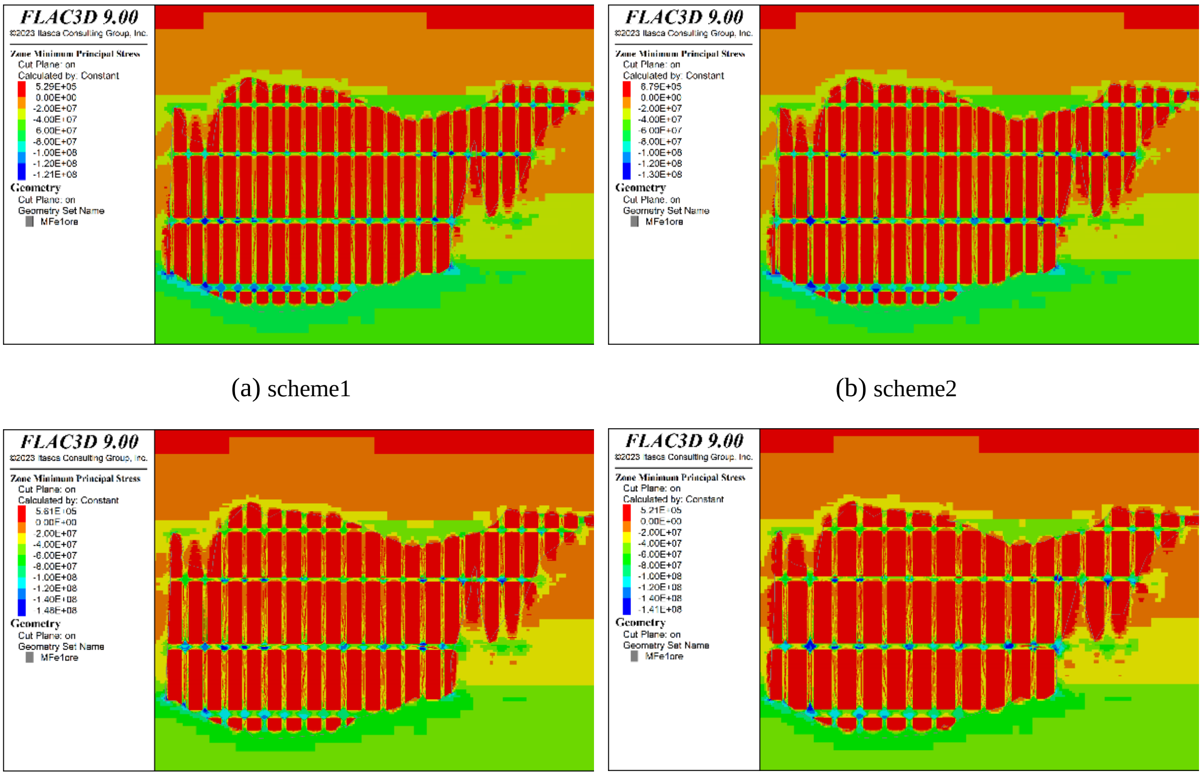

(a) scheme1 (b) scheme2

(c) scheme3 (d) scheme4

Fig. 8 stress redistribution cross-sectional view

There is a local stress concentration phenomenon on the right side of No. 1 horizontal ore pillar. A cross-sectional view reveals that the thickness of the ore body gradually decreases at this location (see Figure 9 for details).

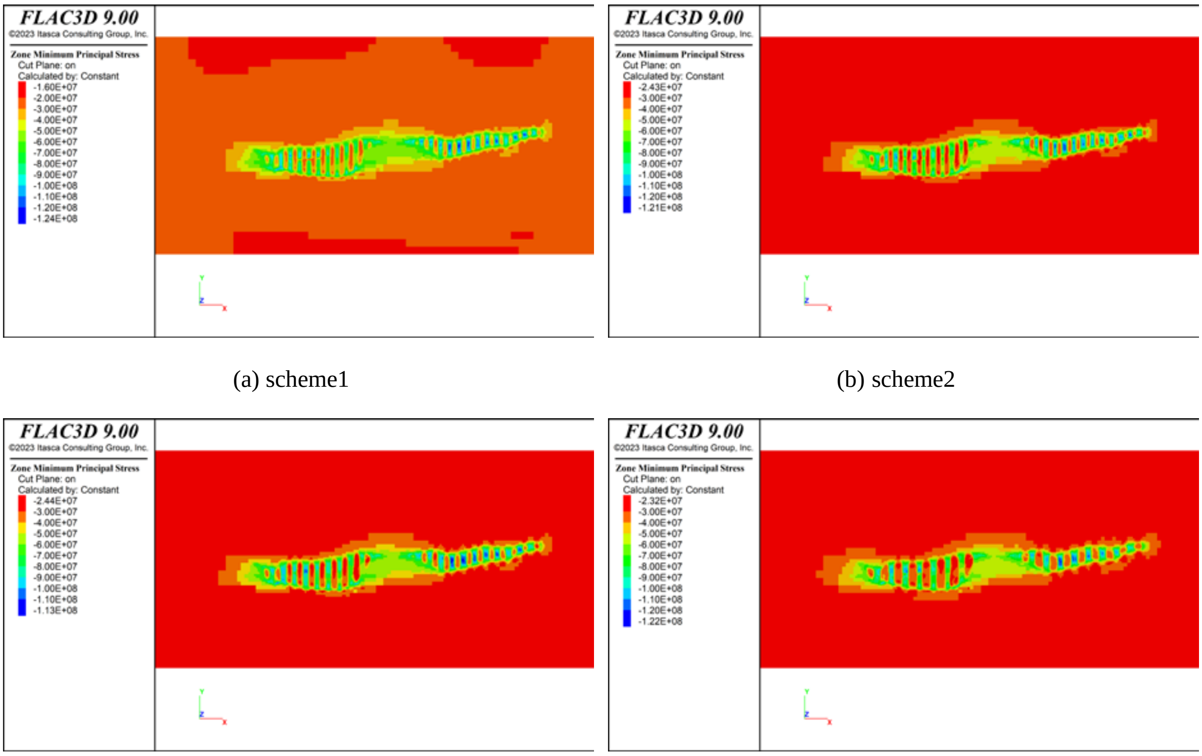

(a) scheme1 (b) scheme2

(c) scheme3 (d) scheme4

Fig. 9 stress redistribution cross-sectional view of 1# horizontal pillar

By integrating the stress redistribution results from the four schemes, it is clear that the thinner the ore body, the more significant the stress concentration. In actual mine production and construction, even within the same mining section, differentiated mining and support schemes must be according to the changes in the ore body's morphology.

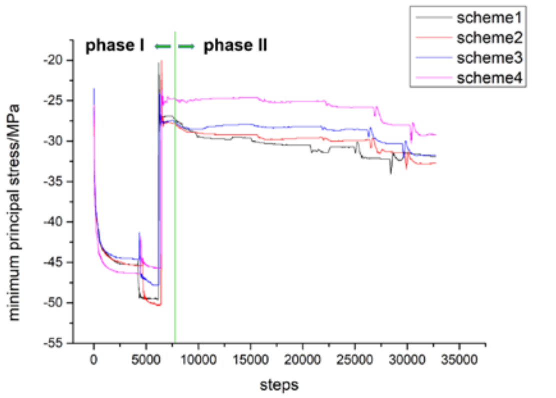

(a) No. 1 horizontal ore pillar(-790m)

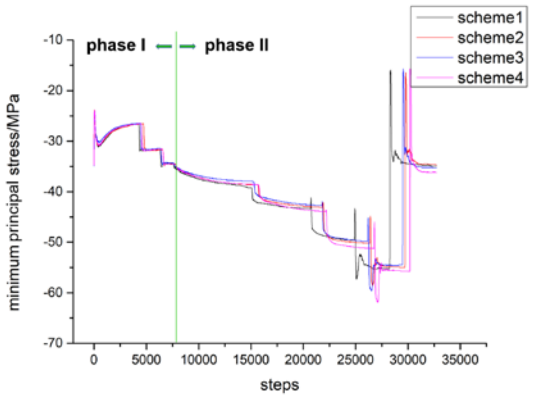

(b) No. 2 horizontal ore pillar(-1030m)

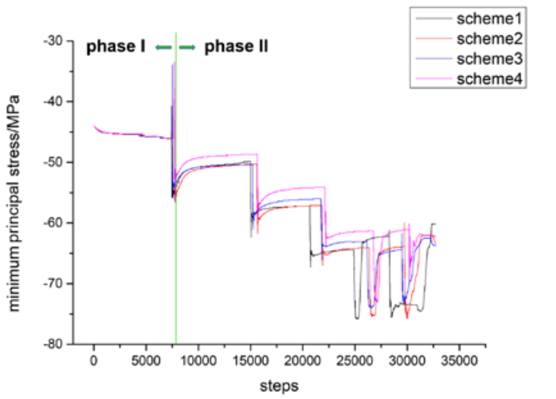

(c) No. 3 horizontal ore pillar(-1350m)

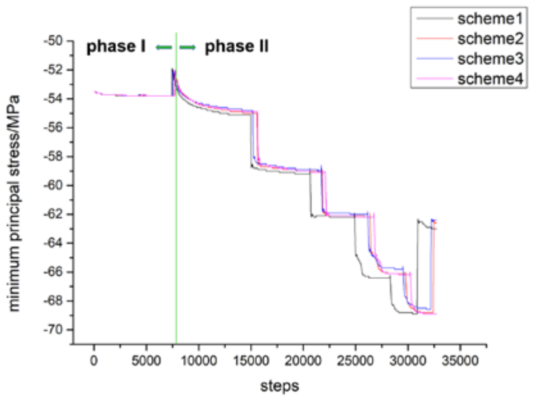

(d) No. 4 horizontal ore pillar(-1680m)

Figure 10 history of minimum principal stress of horizontal pillars

Figure10 shows the history of the minimum principal stress of the horizontal pillars. The No. 1 horizontal ore pillar experienced stress increase decrease in Phase I and gradually stabilized in Phase II, indicating that the backfilling mining in Phase II had little impact on it. The No. 2 horizontal ore pillar showed a trend of stress concentration in Phase I. In Phase II, deep mining lead to a stress reduction effect, and the stress gradually returned to its initial level. The No. 3 horizontal ore pillar continuously exhibited a stress-concentration trend, with the stress eventually stabilized around 60 MPa and a stress-concentration factor of approximately 1.1. The No. 4 horizontal ore pillar also continuously showed a stress-concentration trend, with the stress stabilizing around 63 MPa and a stress-concentration factor of about 1.2.

3.2.3 Plastic zones

Fig.11 illustrates the distribution of plastic zones after the final mining is completed for the four schemes. The red plastic zone "shear-n shear-p" indicates that the area has undergone shear failure during the stress redistribution process, and the shear stress still exceeds the shear strength, suggesting a potential for actual ore pillar failure. The dark green plastic zone "shear-n shear-p tension-p" indicates that the area has experienced both shear and tensile failure during the stress redistribution process, and the shear stress still exceeds the shear strength, also indicating a potential for actual ore pillar failure. The gray plastic zone "shear-p" indicates that the area has suffered shear stress failure during the stress redistribution process. However, after re-equilibrium, the tensile stress does not exceed the shear strength, suggesting that the ore pillars can generally remain stable. The light yellow plastic zone "shear-p tension-p" indicates that the area has experienced both shear and tensile failure during the stress redistribution process. After re-equilibrium, neither the tensile stress exceeds the tensile strength, meaning the ore pillars can generally remain stable. The light green plastic zone "tension-n shear-p tension-p" indicates that the area has undergone both shear and tensile failure during the stress redistribution process, and the tensile stress still exceeds the tensile strength, suggesting a potential for actual ore pillar failure. The mustard-colored plastic zone "tension-p" indicates that the area has experienced tensile stress failure during the stress redistribution process. After re-equilibrium, the tensile stress does not exceed the tensile strength, indicating that the ore pillars can generally remain stable.

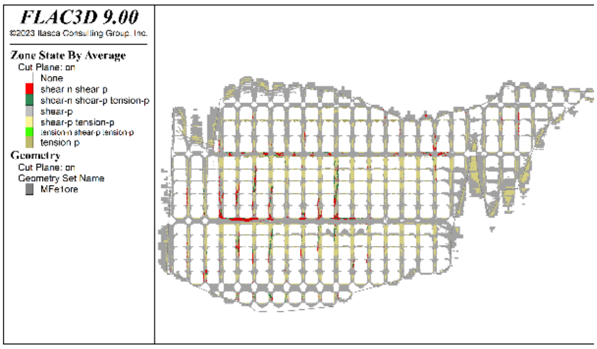

(a) scheme1

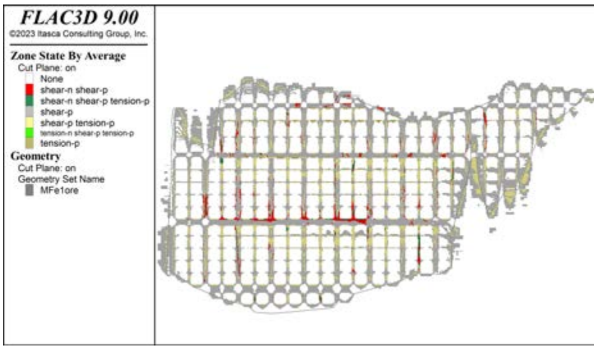

(b) scheme2

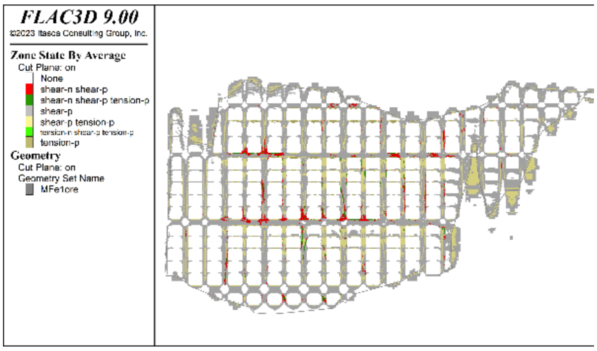

(c) scheme3

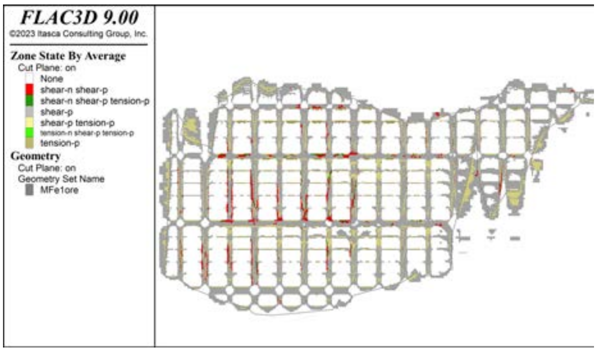

(d) scheme4

Fig. 11 plastic zone state

Based on the cross-sectional views of the plastic zones of the four schemes, it can be observed that: the No. 4 horizontal ore pillar has no areas currently experiencing plastic failure as the mining height is only 60m. The No. 1 horizontal ore pillar has a very small area of plastic failure occurring in the thicker part of the ore body, but it is not continuous, indicating a low risk of failure. Both the No. 2 and No. 3 horizontal ore pillars have sporadic areas of plastic failure. Additionally, in the region with a larger thickness of ore body between the No. 2 and No. 3 horizontal ore pillars, there are also many areas experiencing plastic failure at the base of the vertical pillars in the panel area. Among the four schemes, Scheme 2 has the least area experiencing plastic failure .

4 Conclusions

This study used numerical simulation methods to analyze the stability of mining fields under four different mining structure layouts. By analyzing the vertical and horizontal displacements, minimum principal stresses, and plastic zones after mining for each scheme, the following conclusions were drawn:

(1) The vertical displacement of horizontal ore pillars is influenced not only by the stope span but also by the width of the inter-panel pillars. Larger stope spans and inter-panel pillar widths tend to increase the vertical displacement of horizontal ore pillars. However, the relationship between them is not simply linear, and the change in inter-panel pillar width has a complex impact on the vertical displacement..

(2) The impact of the second-phase mining on the stress redistribution in the shallow part is positively correlated with the burial depth. Although deep mining changes the stress state, overall, its impact on the stress concentration of horizontal ore pillars is relatively small. However, potential impacts on the stability of ore pillars due to stress changes still need to be considered in the design of deep mining.

(3) The thickness of the ore body significantly affects the degree of stress concentration. The thinner the ore body, the more pronounced the stress concentration. In actual mine construction and production, it is necessary to formulate differentiated designs and safety measures according to the

occurrence characteristics of the ore body, such as thickness changes and dip angles, to ensure safe and efficient mining..

(4) A comprehensive comparison of displacement, stress, and plastic zones shows that Scheme 2 has significant advantages. It performs well in controlling displacement, reducing stress concentration, and minimizing the area of plastic failure. It takes into account both mining safety and resource recovery rates and is a superior choice. In actual production, based on Scheme 2, flexible adjustments and optimizations can be made according to on-site actual situations, such as changes in geological conditions and the performance of mining equipment, to achieve sustainable mining of the mine.

Future research can be further expanded to consider the coupled effects of multiple factors, such as groundwater, rock temperature, and dynamic influences, on the stability of deep mining, so as to improve the theoretical and technical system of deep iron ore mining.

Acknowledgement

This work has received funding support from National Key R&D Program of China (No.2023YFC2907201).

References

Zhao, X., Zhou X. (2022) Design Method and Application of Stope Structure Parameters in Deep Metal Mines Based on an Improved Stability Graph. Minerals 13(2). DOI: 10.3390/min13010002.

Zhou, X., Zhao, X. (2023) Stope Structural Parameters Design towards Green and Deep Mining: A Review. Processes, 11(11). DOI:10.3390/pr11113125

Qian, J., Xu W., (2024) Optimization of ore pillar recovery based on weighting combined with uncertainty measurement theory. Journal of Geophysics and Engineering 21(6):1822–1833. DOI:10.1093/jge/gxae108

Andrade L., Dimitrakopoulos R. (2024) Integrated stochastic optimisation of stope design and long-term production scheduling at an operating underground copper mine. Int J Min Reclam Environ, 38:619-41. DOI:10.1080/17480930.2024.2337499

Zhang, Q., Huang, M., J. (2024) A Simulation Analysis of the Stability of Tall and Collapse-Prone Stopes: A Case Study of the Dongguashan Copper Mine. Applied Sciences, 14(22), 10608. DOI:10.3390/app142210608

Saadat, M., Khishvand, M. (2024) FLAC3D Simulation of Caving Mechanism and Strata Fracture Response in Underground Mining. Mining, 4(4), 818-840. DOI:10.3390/mining4040046